

Article

The Importance of Accounting for Atmospheric Effects in the Application of NDVI and Interpretation of Satellite Imagery Supporting Archaeological Research: The Case Studies of Palaepaphos and Nea Paphos Sites in Cyprus

Athos Agapiou ^{1,*}, Diofantos G. Hadjimitsis ¹, Christiana Papoutsas ¹, Dimitrios D. Alexakis ¹ and George Papadavid ^{1,2}

¹ Department of Civil Engineering and Geomatics, Faculty of Engineering and Technology, Cyprus University of Technology, 2-6, Saripolou Str., 3603 Limassol, Cyprus; E-Mails: d.hadjimitsis@cut.ac.cy (D.G.H.); christiana.papoutsas@cut.ac.cy (C.P.); dimitrios.alexakis@cut.ac.cy (D.D.A.)

² Agricultural Research Institute, Ministry of Agriculture, Natural Resources and Environment, 1516 Nicosia, Cyprus; E-Mail: papadavid@arinet.ari.gov.cy

* Author to whom correspondence should be addressed; E-Mail: athos.agapiou@cut.ac.cy; Tel.: +357-2500-2471; Fax: +357-2500-2661.

Received: 20 September 2011; in revised form: 14 November 2011 / Accepted: 15 November 2011 / Published: 2 December 2011

Abstract: This paper presents the findings of the impact of atmospheric effects when applied on satellite images intended for supporting archaeological research. The study used eleven multispectral Landsat TM/ETM+ images from 2009 until 2010, acquired over archaeological and agricultural areas. The modified Darkest Pixel (DP) atmospheric correction algorithm was applied, as it is considered one of the most simple and effective atmospheric corrections algorithm. The NDVI equation was applied and its values were evaluated before and after the application of atmospheric correction to satellite images, to estimate its possible effects. The results highlighted that atmospheric correction has a significant impact on the NDVI values. This was especially true in seasons where the vegetation has grown. Although the absolute impact on NDVI, after applying the DP, was small (0.06), it was considered important if multi-temporal time series images need to be evaluated and cross-compared. The NDVI differences, before and after atmospheric correction, were assessed using student's t-test and the statistical differences were found to be significant. It was shown that relative NDVI difference can be as much as 50%, if

atmosphere effects are ignored. Finally, the results had proven that atmospheric corrections can enhance the interpretation of satellite images (especially in cases where optical thickness of water vapour is minimized ≈ 0). This fact can assist in the detection and identification of archaeological crop marks. Therefore, removal of atmospheric effects, for archaeological purposes, was found to be of great importance in improving the image enhancement and NDVI values.

Keywords: atmospheric correction; modified darkest pixel algorithm; crop marks; vegetation indices

1. Introduction

Many applications of Remote Sensing Archaeology have used multi-temporal satellite imagery for the detection of sub-surface archaeological remains [1-6], monitoring of archaeological sites and their surroundings [7,8], or for risk assessment analysis [9]. In cases of detection of buried archaeological remains, vegetation crop marks, which can be recognized from air/space, are often used.

Vegetation crop marks may be formed in areas where vegetation cover shallow sub-surface archaeological remains. In areas of archaeological interest, the soil tends to retain different percentages of moisture compared to the rest of the crops in the area without any archaeological remains. That means that if vegetation grows over a ditch, especially during periods when water stress develops, the crop growth is likely to be enhanced due to the fact that the topsoil holds more moisture than in the surrounding context. This phenomenon can be recorded from the air (satellite images, aerial photos) and is generally referred to as positive crop mark. However, in cases where there is not enough moisture in the retentive soil and there is a lack of available water for evapotranspiration (vegetation grown above building remains or compacted ground), the developed marks are characterized as negative crop marks and are generally less common than the positive ones [10]. Furthermore, the evolution of crop marks can be a combination of different factors and parameters, such as, moisture availability, the availability of dissolved nutrients to the crops at crucial growing times and periods, for the plant, the crop, the soil type and finally the soil depth [11].

In such studies, vegetation indices have been widely used for the detection of archaeological remains through the enhancement of crop marks. The NDVI equation is the most known index applied in different archaeological areas of the world [12-14]. Although satellite imagery and vegetation indices (e.g., NDVI) are used for the detection of crop marks, atmospheric corrections are often not applied in such studies. However, as Lillesand *et al.* [15] argued, satellite images need to be atmospherically corrected before being subjected to any post-processing techniques. The aim of this study is to validate atmospheric correction methodologies for the purposes of detecting archaeological remains and to assess their importance for crop marks detection.

2. Atmospheric Correction

2.1. Background

In the context of digital analysis of remotely sensed data, pre-processing is generally characterized by two types of data correction: (1) radiometric pre-processing, which addresses variations in the pixel intensities (digital numbers, DN); and (2) geometric correction, which addresses errors in the relative positions of pixels, mainly due to the sensor viewing geometry and terrain variations. Radiometric corrections are distinguished between calibrations, de-striping approaches, atmospheric corrections and removal of data errors or flaws. Radiometric correction is considered to be a more difficult technique than geometric correction since the distributions and intensities of these effects are often inadequately known. Despite the variety of techniques used to estimate the atmospheric effect, the atmospheric correction remains a difficult task in the pre-processing of image data. Furthermore, based on the target under investigation, its impact is an important issue in the retrieval of true and correct outcomes.

The effects of the atmosphere on spectral signatures and vegetation indices have become an important issue in relevant scientific literature since the 1980s (e.g., [16]). Atmosphere is a primary source of noise for accurate measurement of surface reflectance with optical remote sensing [17-19]. Atmospheric effects are a result of molecular scattering and absorption, and influence the quality of the information extracted from remote sensing measurements, such as, vegetation indices. Such errors, caused by atmospheric effects, can increase the uncertainty up to 10%, depending on the spectral channel [20]. Hadjimitsis *et al.* [21] highlighted the importance of considering atmospheric effects when several vegetation indices, such as NDVI were applied to Landsat TM/ETM+ images for agricultural applications. In their study a mean difference of 18% for the NDVI was recorded before and after the application of darkest pixel method.

Therefore, removal of the atmospheric effects is an important pre-processing step required in many remote sensing applications, since it is needed to convert the at-satellite spectral radiances of satellite imagery to their at-surface counterparts [22,23]. Moreover, if an image is to be used for change detection and monitoring purposes, it is essential that adequate atmospheric and radiometric processing be applied, in order to bring all scenes to a common radiometric datum.

Several atmospheric correction algorithms are found in the literature, ranging from simple to sophisticated [24-26]. Hadjimitsis *et al.* [27] classified these algorithms into the following two categories:

- Category (A): Absolute corrections (corrections that lead to surface reflectance). This category can be subdivided into two sub-categories: image-based atmospheric corrections (for example, Darkest Pixel, Covariance Matrix method) and corrections using independent data for atmospheric optical conditions (including *in situ* measurements or historical records) using physical-based algorithms;
- Category (B): Relative corrections (corrections that do not produce values of surface reflectance).

The advantage of the image-based algorithms is the fact that they do not require any ground data during satellite overpass [28]. One of the simplest, fully-imaged based, is the Darkest Pixel (DP)

algorithm, categorized in Category (A). The DP principle is based on the assumption that most of the signal reaching a satellite sensor from a dark object, such as, deep inland water bodies (as in the case of the Asprokremmos Dam followed in this study) is contributed to by the atmosphere at visible wavelengths and on the assumption that the near-infrared and middle infrared image data are free of atmospheric scattering effects [28]. Therefore, the pixels from dark targets are indicators of the amount of upwelling path radiance in that band. The atmospheric path radiance adds to the surface radiance of the dark target, giving the target radiance at the sensor. The surface reflectance of the dark target, for the DP algorithm, is approximated to have zero surface reflectance. A modified adaptation of the DP method is to assume a known non-zero surface reflectance of the dark target based on ground truth data (e.g., spectroradiometric measurements).

Other than water bodies, atmospheric effects, account for the majority of the at-satellite measured radiance in the visible bands [29], and therefore such targets provide an opportunity to assess the effectiveness of the varying atmospheric correction methods [30,31]. This has been shown by Hadjimitsis *et al.* [25], who provided a critical assessment of the effectiveness of most of the available algorithms using Landsat TM satellite imagery and *in situ* spectroradiometric measurements. It was found that the DP method provided a reasonable correction in Landsat TM bands 1, 2, and 3, at least for cloud-free scenes [25]. It has been shown by other researchers [27,32,33] that the DP is the most effective atmospheric correction. The effectiveness of the DP in the NIR band must be taken into consideration in the cases where water vapor absorption is significant [27]. Forster [34] argues that the water vapor thickness is very small for wavelengths less than 0.7 μm but should be taken into account for longer wavelengths such as NIR.

In many archaeological applications, there is a need to use, not only up-to date satellite imagery but, archived multi-temporal data as well. Therefore, the use of physical-based atmospheric correction (Category (A)) can be very difficult to apply, since auxiliary data may not exist for the case study. Moreover, image-based algorithms can be performed easier, even to archive data, regardless of satellite sensor and satellite characteristics.

In this study, an image-based atmospheric algorithm was applied using ground spectroradiometric data acquired over a water body (Asprokremmos Dam). In addition, meteorological data were acquired in order to retrieve optical thickness due to water vapor and to validate the atmospheric correction results. The results were compared to those calculated without removing atmospheric effects (apparent reflectance). For this reason NDVI diagram for a whole phenological cycle of barley crops was drawn and evaluated. Lastly, the results were assessed using visual interpretation of archaeological crop marks.

2.2. Spectral Reflectance (ρ)

The apparent reflectance model is used to correct the digital numbers of the satellite image from solar radiance and sun zenith angle effect. However, this model does not take into consideration any effects occurring from atmospheric scattering and absorption, or from topographic effects. For Landsat TM/ETM+ images calibration is performed based on Equation (1). All the necessary metadata were acquired for each image from the metadata header file:

$$L_{\text{sat}} = [(L_{\text{max}\lambda} - L_{\text{min}\lambda})/Q_{\text{calmax}}] \times Q_{\text{cal}} + L_{\text{min}\lambda} \quad (1)$$

where:

L_{sat} : apparent spectral radiance at satellite sensor ($W \cdot m^{-2} \cdot ster^{-1} \cdot \mu m^{-1}$),

$L_{max\lambda}$ and $L_{min\lambda}$: the calibration constants, ($W \cdot m^{-2} \cdot ster^{-1} \cdot \mu m^{-1}$),

Q_{calmax} : the maximum quantized calibrated pixel value and

Q_{cal} is the digital number of the image.

Following the correction of the Digital Numbers of the images, from the solar radiance effect, the next step was to calibrate the images from the sun zenith angle effect as well. Therefore, to convert the at-satellite radiance values into at-satellite reflectance, using the solar irradiance at the top of the atmosphere, sun-earth distance correction and solar zenith angle Equation (2) was employed:

$$\rho = (\pi \times L_{sat} \times d^2) / ESUN_{\lambda} \times \cos\theta_s \quad (2)$$

where:

ρ : spectral reflectance at the surface (%),

d : earth-sun distance in Aus,

$ESUN_{\lambda}$: solar spectral irradiance on a surface perpendicular to the sun's ray outside of the atmosphere ($W \cdot m^{-2} \cdot \mu m^{-1}$) and

$\cos\theta_s$: cosine of solar zenith angle.

2.3. Modified Darkest Pixel Atmospheric Correction Based on Spectroradiometric Measurements

The modified Darkest Pixel (DP) method [25] was applied in the current study. The surface radiance of the dark targets is assumed to have approximated zero surface radiance or reflectance [27]. Instead of assuming $L_{darkest}$ to be zero value, the modified DP considers the 'true' ground radiance or reflectance value over dark targets as the $L_{darkest}$. Therefore, the spectral reflectance is given by Equation (3):

$$\rho = (\pi \times (L_{sat} - L_{darkest\ target}) \times d^2) / ESUN_{\lambda} \times \cos\theta_s \quad (3)$$

where:

$L_{darkest}$ = Radiance at the darkest target.

The modified DP method applied in this study is based on the assumption that the dark target radiance is not equal to zero since dark targets such as inland water bodies (lakes, reservoirs, dams) are not fully black targets. Therefore, *in situ* measurements are needed in order to measure the "truth" reflectance of the darkest target. For the study area of Palaepaphos, a nearby large inland water body, the Asprokremmos Dam, was selected as the suitable selected dark target. Field spectroradiometric measurements at Asprokremmos Dam were acquired in order to retrieve the surface 'true' reflectance or radiance values (*i.e.*, $L_{darkest}$).

3. Study Areas

For the purposes of this study, two cultivated areas from known archaeological areas (Arkalon-Marhcello, Sites 1–2), and one traditionally agricultural area (Mourokambos, Site 3), have been selected as indicated in Figure 1. Furthermore, the crop mark of the buried ancient amphitheatre

of Nea Paphos (Site 4) was used for the evaluation of the importance of atmospheric corrections. Finally, the Asprokremmos Dam (Site 0) was used for the application of the modified DP algorithm.

Palaepaphos is situated on the SW coast of the island and was selected as a case study area. Palaepaphos is an extensive archaeological landscape and is listed in the World Heritage List of UNESCO since many important monuments, dating from the Chalcolithic period until today, are situated there. Its few visible secular and sepulchral monuments and its famous open-air sanctuary to an aniconic deity, known as Aphrodite, are scattered over an area of two square kilometers [35].

In this area, archaeological excavations have systematically been carried out, while in the past few years, systematic foot surveys and geophysical surveys have also been performed. Arkalon and Marhcello localities (Sites 1 and 2 respectively) are located in the Palaepaphos archaeological site and have attracted the interest of the archaeologists in recent years [14,36-38].

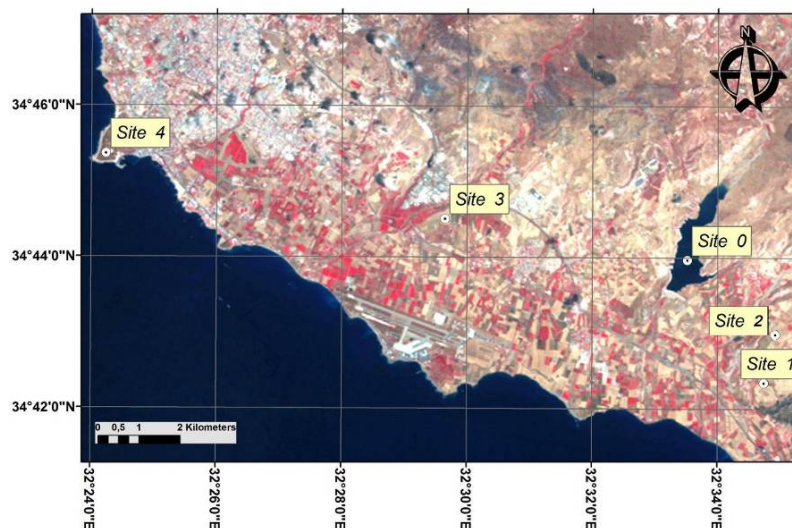
The surroundings of Palaepaphos are also considered to be an important agricultural area for Cyprus. At the Mourokambos locality (Site 3), barley crops have been traditionally cultivated. It should be mentioned that during 2009–2010 (the period studied) in both sites (Palaepaphos and Mourokambos) barley crop was cultivated.

Moreover, Palaepaphos and Mourokambos areas are in close vicinity with the Asprokremmos Dam, the second largest dam in Cyprus (Site 0), which was used for the modified DP algorithm.

Nea Paphos (Site 4), according to written sources, was founded at the end of the 4th Century by Nicocles, the last king of Palaepaphos. In the beginning of the 3rd Century BC when Cyprus became part of the Ptolemaic Kingdom, which had its capital in Alexandria, Nea Paphos became the center of Ptolemaic administration in Cyprus. Until the end of the 2nd Century BC, the site became the political and economical centre of the region and therefore the Ptolemies made Nea Paphos the capital of Cyprus.

Nea Paphos regained some of its glamour during the Byzantine and Medieval periods but from the Venetian period and onwards, the coastal settlement of Nea Paphos was abandoned and the population moved further inland where the present town of Paphos was established [39].

Figure 1. Case study areas mentioned in the text. Site 0 is the Asprokremmos Dam, Sites 1 and 2 are the archaeological sites of Palaepaphos (Arkalon and Marchello localities), Site 3 is the Mourokambos agricultural field and Site 4 is the Nea Paphos archaeological site.



4. Methodology

4.1. Overall Methodology

For the objective of this study, Landsat TM/ETM+ multispectral images have been collected from USGS Glovis. The images were geometrically corrected and then, the apparent reflectance was calculated. In this step, the digital numbers (DN) of the images were converted into units of radiance and then reflectance. Following that, atmospherically corrected images were produced, using ground spectroradiometric measurements over the Asprokremmos Dam. These measurements were collected periodically from April to October (2010).

The next step included the calculation of the NDVI index over the Palaipaphos archaeological site. The NDVI values were compared both for the archaeological and non-archaeological site (agricultural areas). In both cases, the same kind of crop was cultivated (barley), while the areas have similar soil and climatic characteristics. Finally, interpretation of the results over the archaeological site of Nea Paphos and the Asprokremmos Dam was performed in order to evaluate atmospheric effects. For this purpose the global minimum and global maximum DN value for each band, for all images dataset, was calculated and then linear histogram enhancement was performed.

4.2. Resources

For the purposes of the study, multispectral Landsat TM/ETM+ satellite images have been used. Next, ground spectroradiometric data from the inland water of the Asprokremmos Dam have been acquired. Finally, meteorological data have been collected for the needs of the atmospheric corrections algorithms. A detail description of the data is provided in the followings chapters.

4.2.1. Satellite Imagery

With the opening of the Landsat archive by the USGS in 2009, a huge amount of images have become available to scientists [40]. Eleven (11) Landsat TM/ETM+ satellite images acquired on 2009 and 2010 were used in this study, to cover the whole life cycle of the barleys crops as shown in Table 1. The ERDAS Imagine v.10 software was used for the pre-processing and post-processing of satellite imagery.

4.2.2. Field Spectroradiometric Data

In this study, a power-engine boat was used to support the *in situ* campaign in the Asprokremmos Dam in Paphos and a Global Position System Garmin GPS72 was used in order to store the selected sampling station [41]. Sampling campaigns started in April 2010 and last until October 2010 including 16 sampling campaigns. A handheld GER-1500 field spectro-radiometer (spectral range covered by the instrument extends from 400 to 1,050 nm) equipped with a fiber optic probe was used, in order to retrieve the spectral signatures of the Asprokremmos Dam (see Figure 2). Reflectance was calculated as a ratio of the target radiance to the reference radiance. The target radiance value is the measured value taken on the surface water of the reservoir and the reference radiance value is the measured value

taken on the standard Spectralon panel, representing the sun radiance, which reaches the earth surface—without atmospheric influence. Figure 3 show typical reflectance values of the dam.

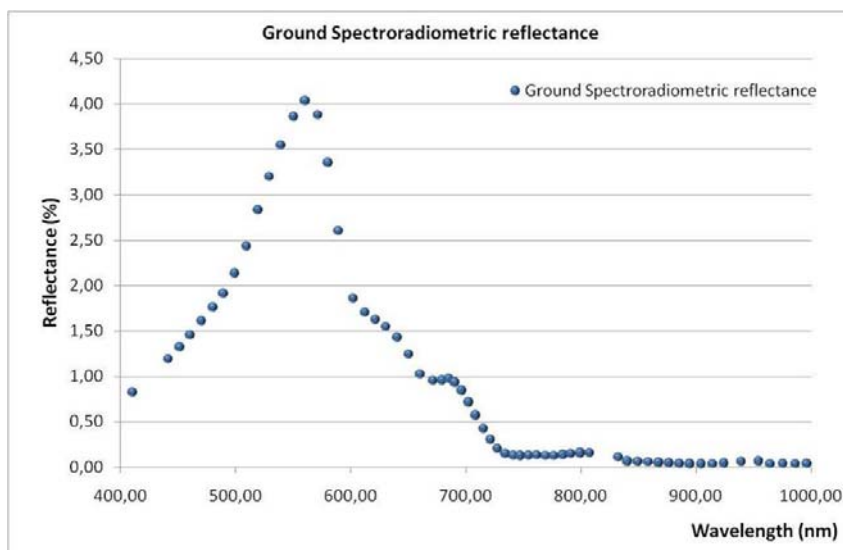
Table 1. Satellite image acquisition dates.

No	Satellite	Sensor	Acquisition Date	Julian Date	Sun Elevation	Sun Azimuth
1	Landsat	TM	21/06/2009	172	65.88	111.03
2	Landsat	ETM+	29/06/2009	180	65.77	111.50
3	Landsat	TM	07/07/2009	188	64.84	111.92
4	Landsat	TM	14/07/2009	195	64.16	113.41
5	Landsat	TM	23/07/2009	204	63.10	116.16
6	Landsat	TM	25/09/2009	268	49.04	145.70
7	Landsat	ETM+	22/12/2009	356	27.96	155.96
8	Landsat	ETM+	07/01/2010	7	28.30	153.70
9	Landsat	ETM+	19/03/2010	78	47.66	140.76
10	Landsat	ETM+	13/04/2010	103	56.66	134.51
11	Landsat	TM	15/06/2010	167	66.48	112.40

Figure 2. GER1500 field spectroradiometer (a) Reference spectroradiometric measurements on the white spectralon panel (b) Target spectroradiometric measurements using a fiber optic probe.



Figure 3. Typical ground spectroradiometric measurements at the Asprokremmos Dam.



4.2.3. Meteorological Data

Meteorological data were provided from the Meteorological Service of Cyprus, in order to search if any significant climatic differences have occurred during the satellite overpass. As it was found (Table 2), the relative humidity during the satellite overpass was similar ($\approx 57\text{--}67\%$) for all days except 19/03/2010 (33%) and 15/06/2010 (77%). Relative humidity and temperature as shown by Forster [34] and by Hadjimitsis and Clayton [30] can be used to provide a measure of the equivalent mass of liquid water or water vapour thickness. Although DP algorithm can be applied without any auxiliary meteorological data, as a fully image-based technique, the authors used these data to investigate any possible water vapour absorption effect in atmospheric correction.

Table 2. Meteorological data from the Paphos airport (Data provided from Meteorological Service of Cyprus).

No	Acquisition Date	Max Temperature	Min Temperature	Temperature 13:00	Rainfall (mm)	Relative Humidity 13:00 (%)
1	21/06/2009	31	20	29.5	0.00	62
2	29/06/2009	28	18	27.8	0.00	68
3	07/07/2009	30	22	29.5	0.00	67
4	14/07/2009	30	21	29.4	0.00	64
5	23/07/2009	32.3	21	32.3	0.00	68
6	25/09/2009	29	19	28.3	0.05	58
7	22/12/2009	20.5	12.9	20.5	0.33	57.4
8	07/01/2010	20.0	9.3	19.6	0.00	63
9	19/03/2010	18.9	7.1	18.5	0.00	30
10	13/04/2010	20.7	11.3	20.6	0.00	67
11	15/06/2010	27.4	19.4	26.7	0.00	77

According to Forster [34] and McClatchey *et al.* [42], optical thickness values of water vapor can be calculated based on relative humidity and temperature. In this case, the partial pressure of water vapour is calculated based at the assumption of ideal gas law. Absorption, due to water vapor for wavelengths lower than $0.7\ \mu\text{m}$, can be ignored [34]. Therefore, the assumption that absorption of water vapor for visible bands of Landsat TM/ETM+ (Band 1: $0.45\text{--}0.52\ \mu\text{m}$; Band 2: $0.52\text{--}0.60\ \mu\text{m}$; Band 3: $0.63\text{--}0.69\ \mu\text{m}$) is zero, was made for the objective of this study. However, optical thickness of water vapor, for the NIR band (Band 4: $0.76\text{--}0.90\ \mu\text{m}$) for Landsat, needs to be calculated as indicated in Table 3. As it was found, the last three images (19/03/2010; 13/04/2010 and 15/06/2010) used in this study had the minimum optical thickness of the water vapor from all dataset. In the rest of the image dataset, the optical thickness ranged from 0.031 to 0.067.

Table 3. Equivalent mass of liquid water for the satellite images used in this study.

No	Acquisition Date	Equivalent Mass of Liquid Water (g/cm ²)	τ_{H_2O}
			(Optical Thickness of Water Vapor) Band 4 (0.76–0.90 μm)
1	21/06/2009	1.70	0.055
2	29/06/2009	1.80	0.058
3	07/07/2009	1.95	0.063
4	14/07/2009	1.95	0.063
5	23/07/2009	2.10	0.067
6	25/09/2009	1.50	0.048
7	22/12/2009	1.00	0.031
8	07/01/2010	1.10	0.034
9	19/03/2010	0.25	0.008
10	13/04/2010	0.30	0.009
11	15/06/2010	0.85	0.026

5. Results

The inland water spectroradiometric measurements (Table 4) have shown that the reflectance values over the Asprokremmos Dam were very low and tend to be nearly zero, especially at the NIR band. In detail blue band has an average reflectance of 1.67% ($\pm 0.44\%$), green band 3.21% ($\pm 0.72\%$), red band 1.07% (± 0.30) and the NIR band 0.09% ($\pm 0.03\%$). According to statistics, standard deviation of the results was less than 1% while for Red and NIR bands (which are often used for vegetations indices) the deviation was less than 0.30%. These results were used for the modified DP algorithm.

Modified DP algorithm was applied for removal of the atmospheric effects using the mean values of the spectroradiometric campaigns. The NDVI index was calculated for Sites 1–3 using atmospherically corrected satellite images and non-atmospherically corrected images. As is indicated in Figure 4, lower values of NDVI can be found in images where no atmospheric correction was applied. Modified DP algorithm tends to give higher NDVI values for all sites selected in this study. The average difference of NDVI values before and after the DP algorithm was calculated to be 0.10. However, the difference in relative values of NDVI before and after the atmospheric correction is estimated to be 25%. This is far less than using DP without any ground measurements (0.16 NDVI mean absolute difference or 32% relative difference).

The difference of NDVI values was assessed using the Student's t-test in order to evaluate the statistical significance of the differences between the two sample means: before and after the atmospheric correction. As it was found t_{observed} for Sites 1–3 ($t_1 = 5.205$; $t_2 = 5.064$; $t_3 = 14.587$) was higher than the $t_{\text{statistical}}$ ($t_{1-3} = 2.228$) for ($n - 1 = 10$) degrees of freedom and at a confidence level of 95%. This implies that NDVI values after the atmospheric correction have a significant statistical difference from the corresponding NDVI values, before the removal of the atmospheric effects.

In the case of Landsat TM or ETM+ satellite images acquired at 15/06/2010, where low water vapor optical thicknesses occurred, the difference of NDVI values before and after the modified DP algorithm is greater (≈ 0.15 absolute difference of NDVI values or 30% relative differences). Concerning DP algorithm, the difference was estimated at 0.30 absolute NDVI difference or 60%

relative difference. These differences might be a result of the low impact of water absorption in the image reflectance.

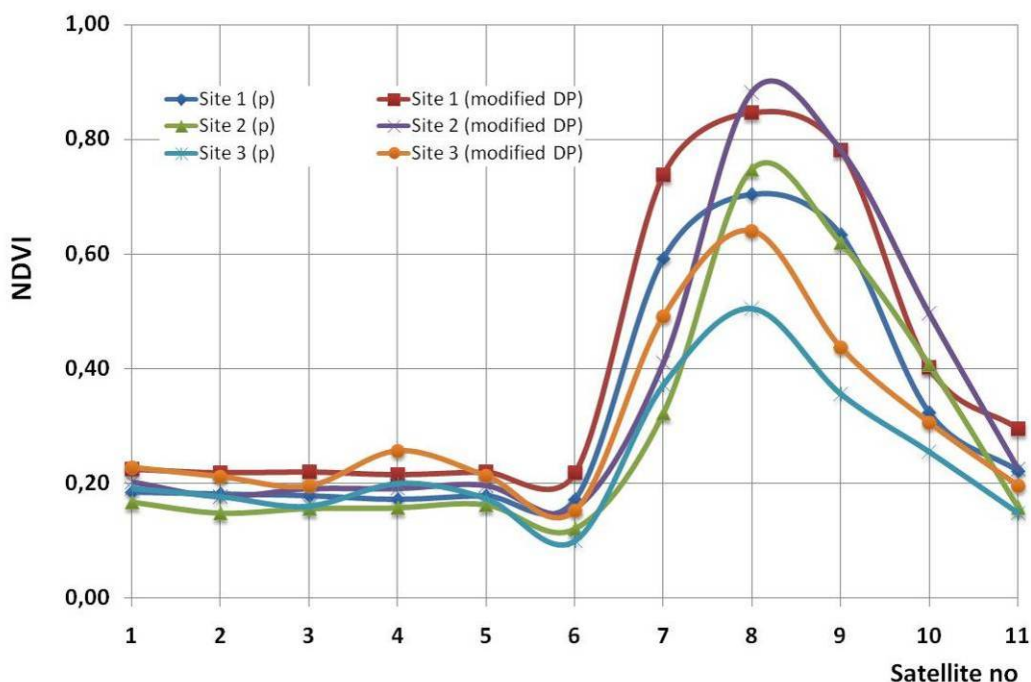
Table 4. Spectroradiometric measurements over the Asprokremmos Dam.

Campaign	Band 1 (%)	Band 2 (%)	Band 3 (%)	Band 4 (%)
1	1.08	2.20	0.70	0.05
2	1.48	2.89	1.08	0.09
3	1.76	3.70	1.39	0.10
4	1.35	3.12	1.14	0.09
5	1.58	3.58	1.28	0.11
6	1.72	3.53	1.24	0.10
7	1.56	3.22	1.10	0.11
8	2.73	4.88	1.52	0.12
9	1.61	2.95	0.80	0.05
10	1.57	2.86	0.82	0.06
11	1.49	2.82	0.78	0.07
12	2.15	3.87	1.17	0.10
13	1.78	3.31	1.05	0.11
14	0.96	1.88	0.54	0.05
15	1.56	2.70	0.93	0.07
16	2.36	3.90	1.62	0.13
Average	1.67	3.21	1.07	0.09
Max.	2.73	4.88	1.62	0.13
Min.	0.96	1.88	0.54	0.05
Std.	0.44	0.72	0.30	0.03

Such differences have also been reported in relevant literature. Indeed, Song and Woodcock [19] argue that, the NDVI calculated from apparent reflectance is the lowest while the NDVI values from different other algorithms (including DP algorithm) are much higher. Moreover, the observed pattern matches the theoretical analysis mentioned by Pinty and Verstraete [43], that atmospheric effects reduce NDVI. Special attention is given in the satellite images, acquired from September to May (No 6–10 in Figure 4), when barley crops were cultivated in the archaeological area of Palaepaphos. As is shown in Figure 4, significant differences might occur in the image interpretation, since NDVI values vary a lot in this period, if there is a need for time-series satellite interpretation.

However, it should be noticed that, although NDVI atmospheric corrected, provide the optimum results due to the removal of all the major radiometric effects, the NDVI values without taking into account the atmospheric effect, tend to give similar results with a variant offset of values in the Y-axes (NDVI values). This is a result of the NDVI equation, since it is a ratio of Red and NIR bands and therefore tends to self-calibrate atmospheric impact. Nevertheless, NDVI cannot minimize atmospheric effects like other indices, such as ARVI and SARVI. Indeed, such indices reduce the influence of the atmosphere by engaging the red-blue channel instead of the red one. ARVI and SARVI indices retrieve information regarding the atmosphere capacity, since compared to the red band, the blue band is much more easily scattered by the atmosphere particles [44].

Figure 4. NDVI values for Site 1 and Site 2 using: (a) reflectance values and (b) after the modified DP algorithm reflectance values were applied.



Evaluation of the importance of atmospheric effects for the detection of archaeological crop marks is a difficult task. In order to evaluate the impact of atmospheric correction at satellite interpretation, the authors selected a known archaeological crop mark, at the Nea Paphos archaeological site (Site 4) and a dark target (Site 0), for visual interpretation. The ancient amphitheatre of Nea Paphos (Figure 5) was selected due to its size, which is detectable from Landsat images ($\approx 3 \times 2$ pixels in Vis and NIR bands).

The maximum and minimum histogram values of each band were estimated for all satellite images (before and after the atmospheric correction) in order to retrieve the \max_{Global} and \min_{Global} . Afterwards, a linear stretch was performed for each band based on these values. Using this simple technique, all scenes were corrected to a common radiometric range (see Figure 6).

Figure 5. Crop mark at the Nea Paphos archaeological site.



Figure 6. $Global_{min}$ and $Global_{max}$ diagram for histogram enhancement.

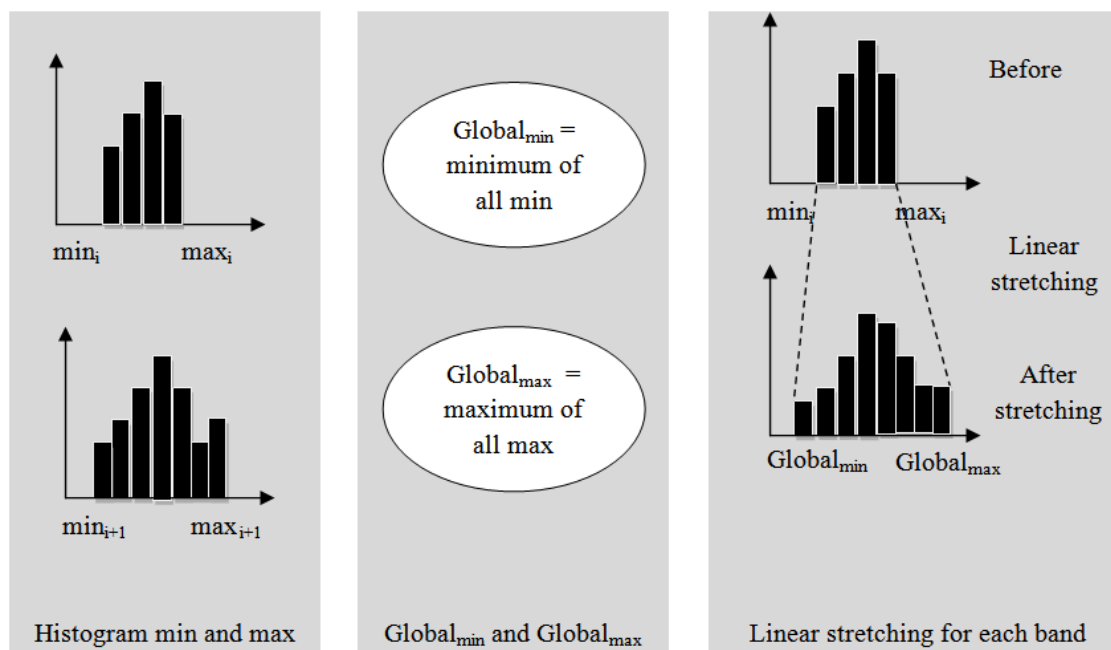


Table 6 indicates the results of the atmospheric correction for each band, at the surroundings of the Asprokremmos Dam. As is shown, the interpretation is improved after the atmospheric effects were removed. This is obvious for all bands and for the false-color images produced (NIR-R-B) by them. Atmospheric corrected images tend to enhance the image histogram and to improve both the final quality and the interpretation of the images. This is very important for remote sensing archaeological research since interpretation is considered to be a helpful tool for the detection of buried archaeological remains through crop marks.

Table 7 shows some of the results before and after the application of modified DP atmospheric correction, at the Nea Paphos archaeological site. Again, the interpretation qualities of the images are slightly improved after the removal of atmospheric effects. The Best photo interpretation quality was found at images with low water vapor optical thickness (19/03/2010; 13/04/2010 and 15/06/2010) for both sites (Nea Paphos and Asprokremmos Dam). On these days, the optical thickness of water vapor was minimum (less than 0.03). Nevertheless, for the rest of the images, where water vapor optical thickness was less than 0.05, the quality of the images after the atmospheric correction was improved. In the case of higher values (e.g., 14/07/2009, water vapor optical thickness = 0.063) the quality was not sufficiently improved.

Table 8 indicates some results before and after atmospheric correction, based on the DP algorithm. In this case, the Asprokremmos Dam was used as the dark target. This methodology assumes that the pixel of the dam with the lowest digital number (DN) or radiance in each band should actually have zero value and therefore its radiometric DN or radiance value will represent the atmospheric additive [27]. As is shown, DP algorithm tends to enhance better archaeological crop marks in contrast with the non-corrected satellite image. Moreover, in the cases of low optical thickness of water vapor values (for example, as the case of the image acquired on 15/06/2010), this enhancement is maximized. However, during the linear stretch application (using the max_{Global} and min_{Global}), it has been found from the image statistics that the image acquired at 15/06/2010 has a reflectance value of 33% for

band 4, which corresponds to the lowest reflectance values from all multi-temporal imagery series. The global maximum value (from all images) was 57%. This caused an over-stretch enhancement to the image, *i.e.*, presence of saturated pixels. However, the effect of the DP atmospheric correction, improves the image significantly, as shown in Figure 8 and discussed later.

Hence, it should be mentioned that DP can be used in cases where “true” dark target is visible in the image and water vapor optical thickness is minimized (≈ 0).

Table 6. Interpretation of the results before and after the atmospheric correction at the Asprokremmos Dam.

		Band 1	Band 2	Band 3	Band 4	NIR-Red-Green
21/06/2009	Before atmospheric					
	After atmospheric					
07/07/2009	Before atmospheric					
	After atmospheric					
14/07/2009	Before atmospheric					
	After atmospheric					

Table 6. Cont.

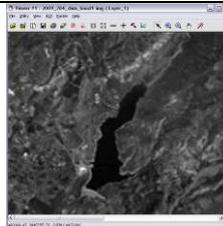
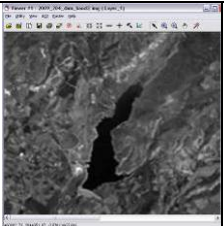
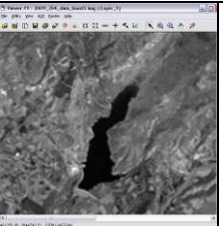

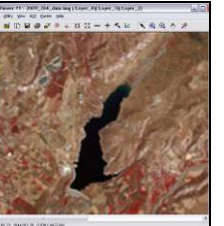
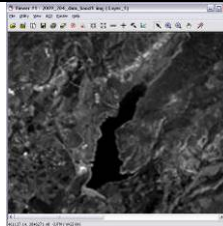
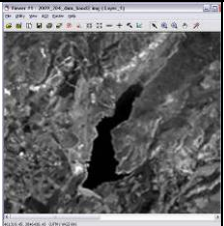
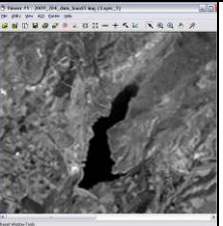

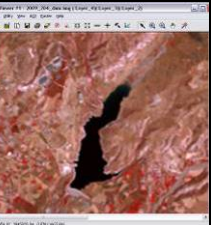
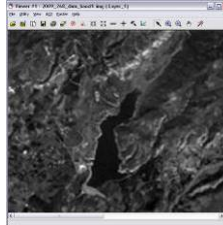
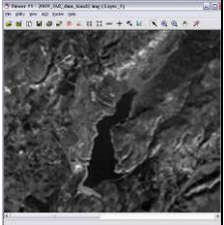
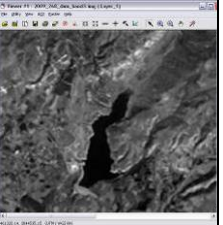
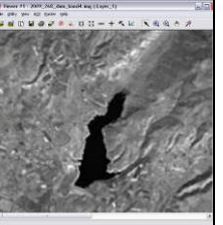

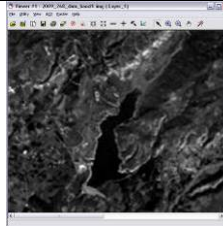
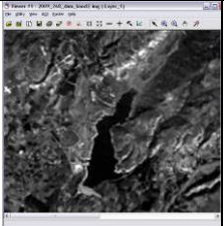
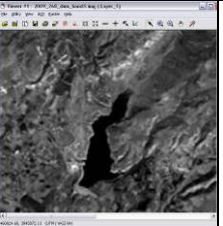
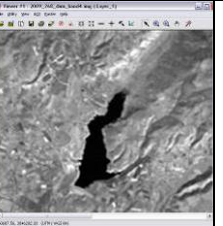
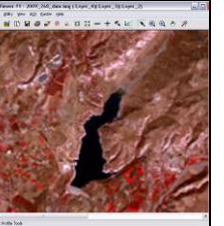
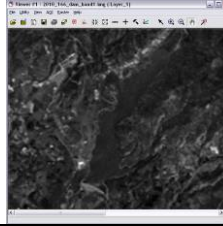
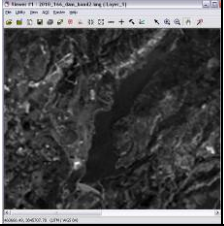
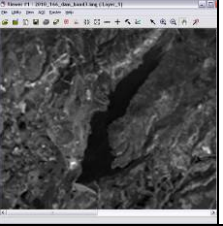

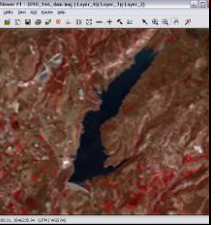
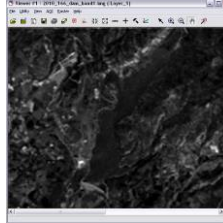
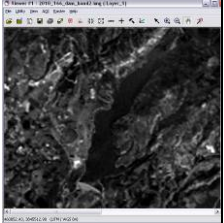
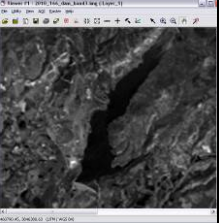
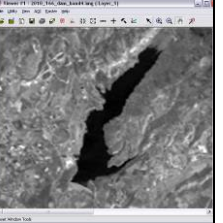
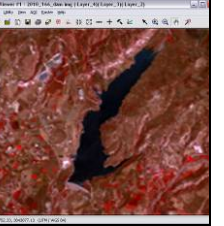
23/07/2009	Before atmospheric					
	After atmospheric					
25/09/2009	Before atmospheric					
	After atmospheric					
15/06/2010	Before atmospheric					
	After atmospheric					

Table 7. Interpretation of the results before and after the modified DP atmospheric correction applied at the Nea Paphos crop mark (the archaeological crop mark in Nea Paphos has been circled, 1st row, 1st image from the left).

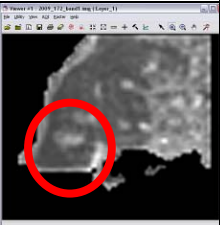
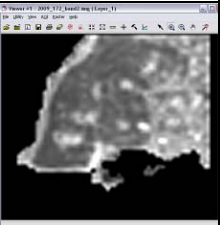
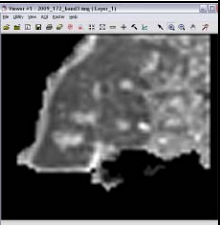
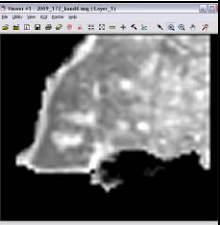
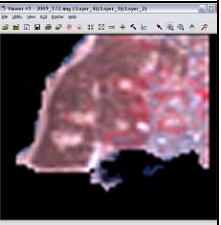
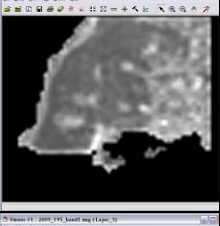
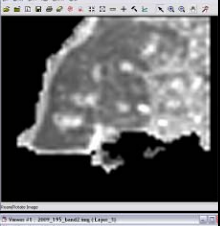
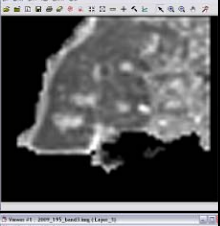
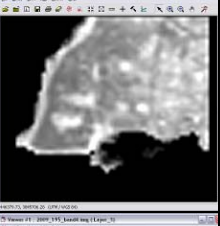
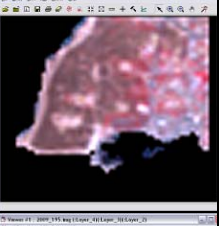
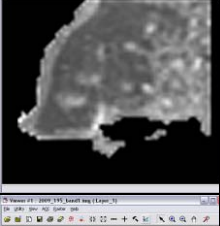
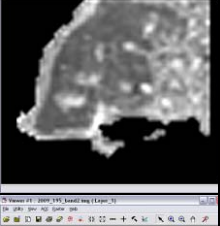
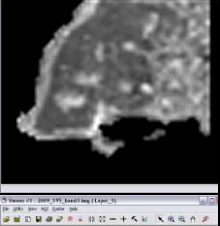
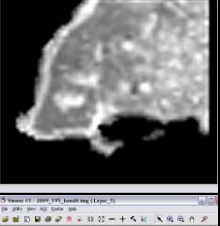
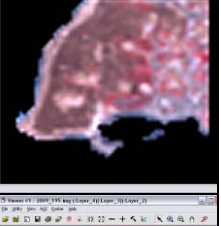
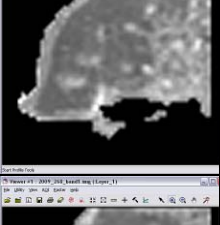
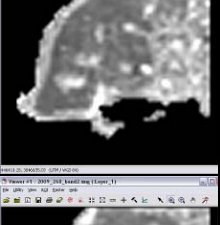
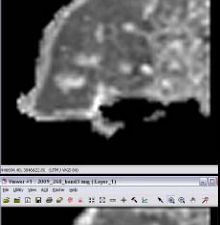
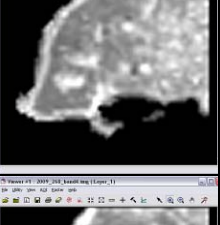
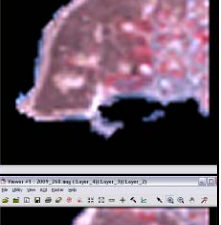
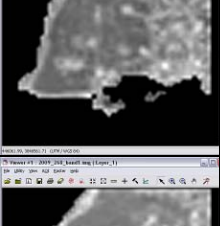
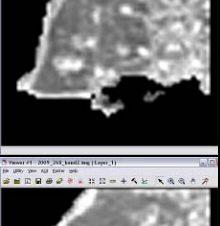
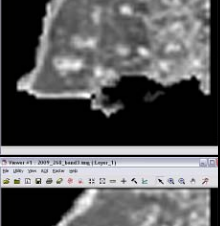
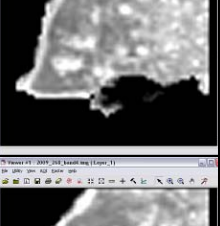
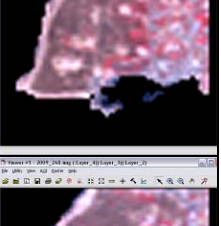



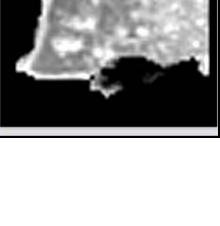

		Band 1	Band 2	Band 3	Band 4	NIR-Red-Green
21/06/2009	Before atmospheric					
	After atmospheric					
14/07/2009	Before atmospheric					
	After atmospheric					
25/09/2009	Before atmospheric					
	After atmospheric					

Table 7. Cont.

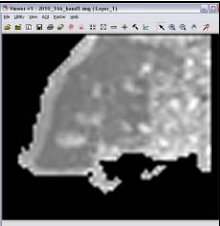
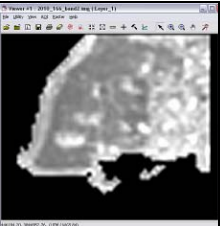
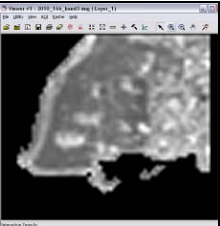
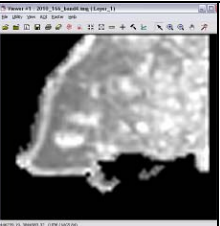
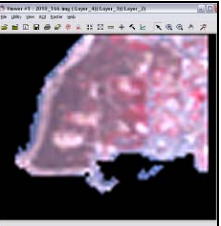
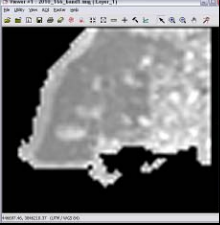
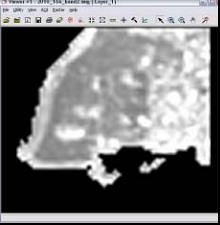
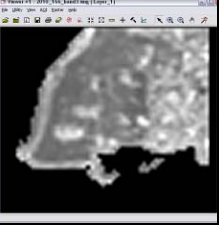
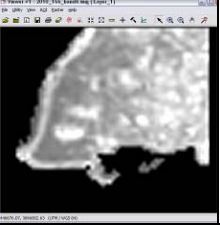
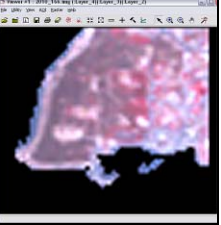
15/06/2010	Before atmospheric					
	After atmospheric					

Table 8. Interpretation of the results before and after the DP atmospheric correction applied at the Nea Paphos crop mark.

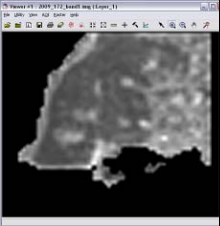
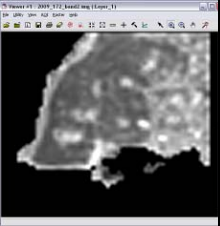
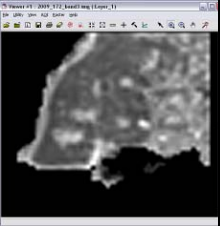
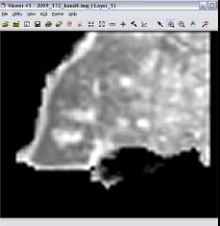
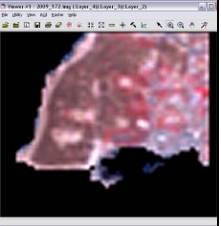
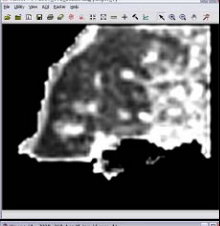
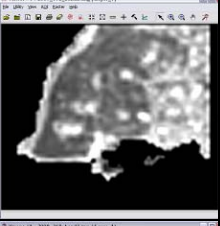
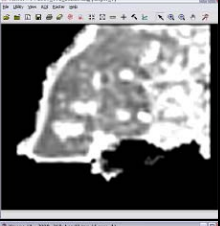
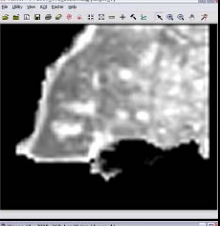
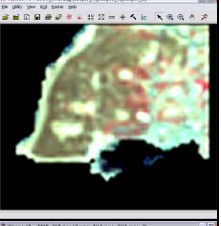
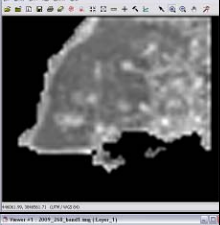
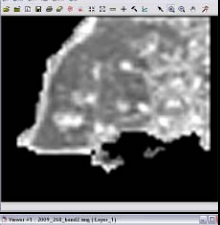
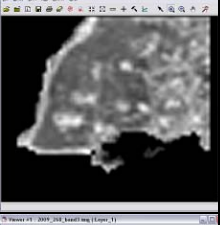
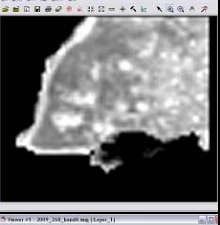
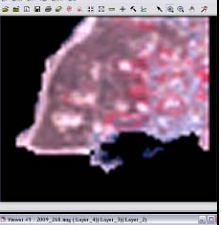

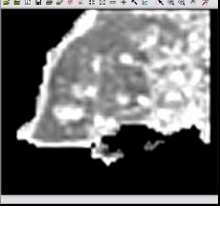
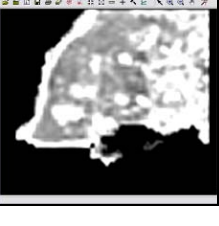

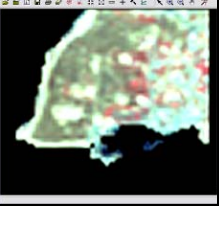
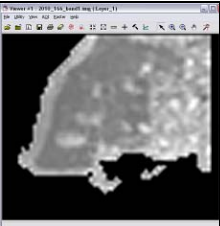
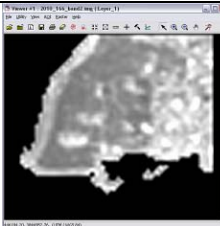
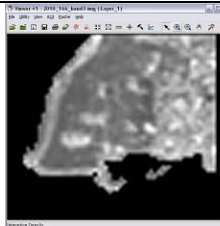
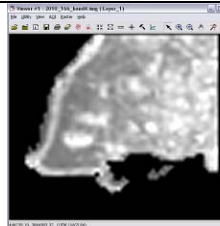
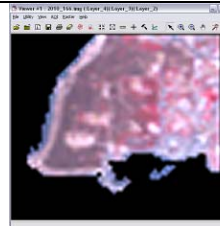
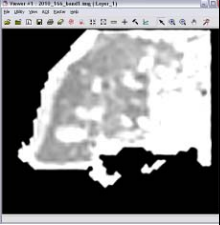
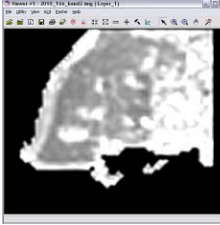
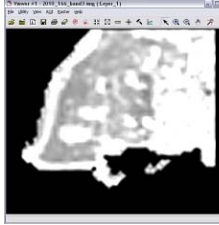
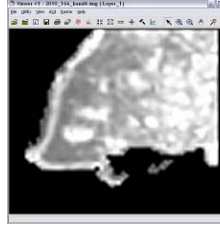
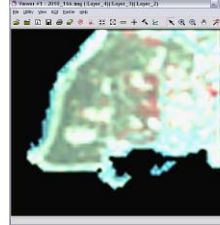
		Band 1	Band 2	Band 3	Band 4	NIR-Red-Green
21/06/2009	Before atmospheric					
	After atmospheric					
25/09/2009	Before atmospheric					
	After atmospheric					

Table 8. Cont.

15/06/2010	Before atmospheric					
	After atmospheric					

In order to evaluate the difference between NDVI values, before and after atmospheric correction, the relative NDVI values after atmospheric correction (percentage relative difference) was plotted against non-atmospheric corrected NDVI values, for all Sites, as shown in Figure 7. As was expected, for Site 0 (dam) a linear correlation (before and after atmospheric correction) was found, since a single value (average from red and NIR bands) was used. Nevertheless, for the rest of the sites, significant differences that are non-linear have been observed. Relative differences for low NDVI values (<0.40) can be as 50% more in cases of atmospheric corrected images in comparison with non-atmospheric images. For higher NDVI values (>0.40) relative differences tend to be smaller (≈20%) (see Table 9). Indeed, the effect of the atmosphere must be taken into consideration since the magnitude of atmospheric effects to the NDVI tends up to 50 % as shown in this study.

Figure 7. Relative NDVI values after atmospheric correction (modified DP) against NDVI values before atmospheric correction.

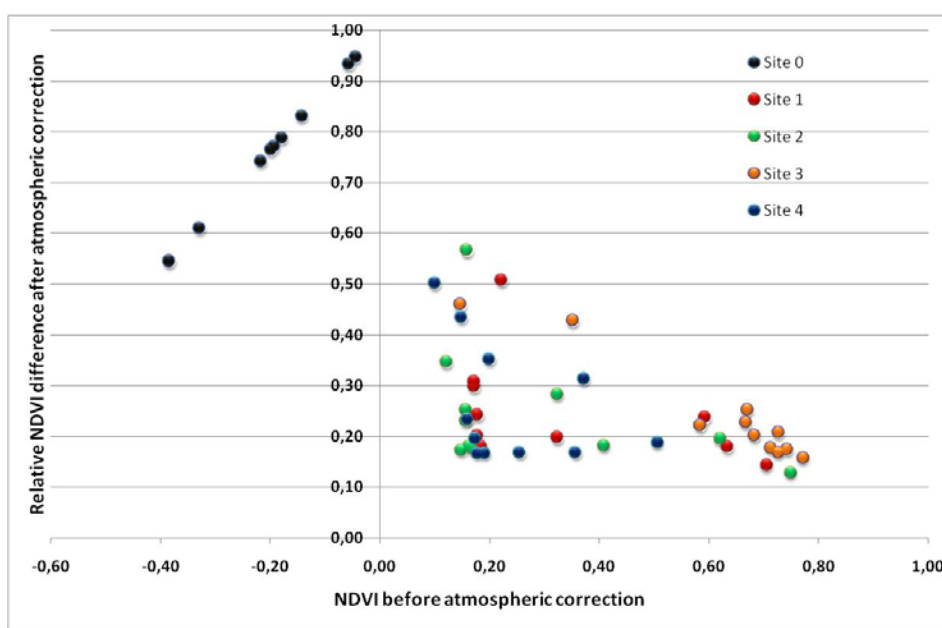
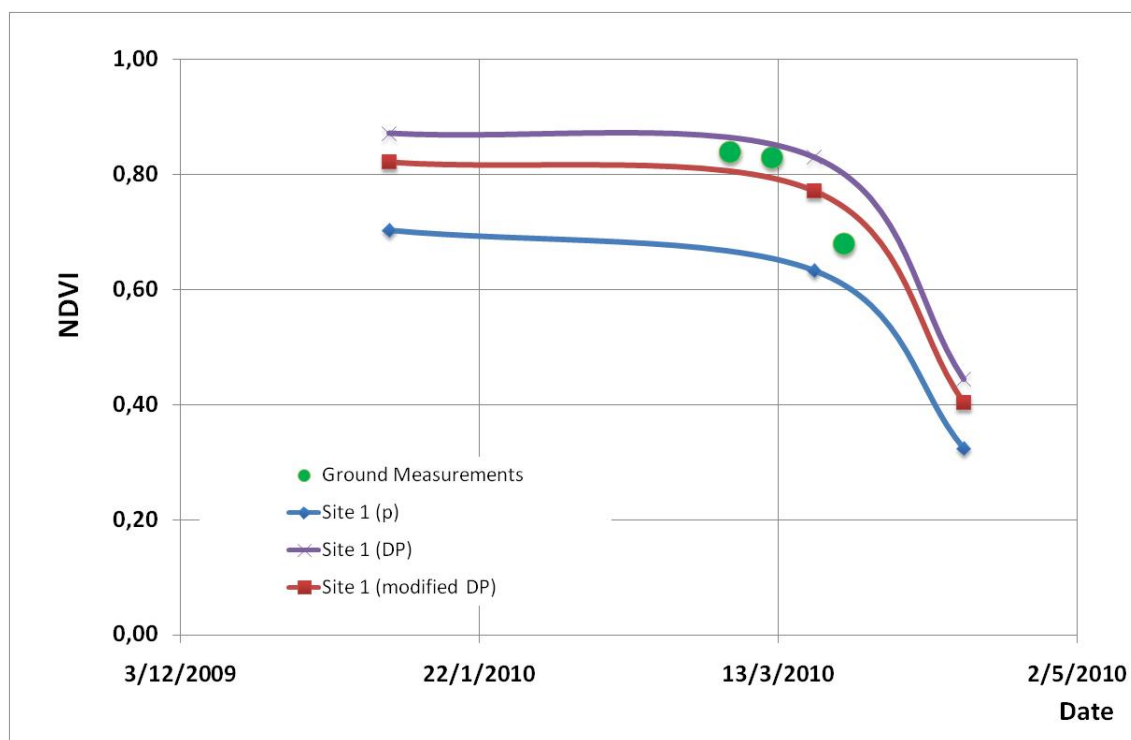


Table 9. Relative NDVI differences for all sites, before and after atmospheric correction (min and max values for each site are underlined).

no	Acquisition Date	Site 0 (before AC)	Site 0 (after A)	Relative Difference in %				
				Site 0	Site 1	Site 2	Site 3	Site 4
1	21/06/2009	-0.217		0.743	0.180	0.178	0.169	<u>0.167</u>
2	29/06/2009	-0.194		0.771	0.178	0.173	0.174	0.168
3	07/07/2009	-0.143		0.831	0.243	0.231	0.252	0.235
4	14/07/2009	-0.057		0.932	0.298	0.252	0.428	0.352
5	23/07/2009	-0.217		0.743	0.200	0.181	0.178	0.197
6	25/09/2009	-0.329	-0.845	0.611	0.309	0.346	0.207	0.501
7	22/12/2009	-0.385		<u>0.545</u>	0.237	0.283	0.227	0.313
8	07/01/2010	-0.383		0.546	<u>0.143</u>	<u>0.129</u>	<u>0.158</u>	0.188
9	19/03/2010	-0.179		0.788	0.180	0.195	0.221	0.169
10	13/04/2010	-0.199		0.765	0.198	0.182	0.201	0.169
11	15/06/2010	-0.045		<u>0.946</u>	<u>0.508</u>	<u>0.566</u>	<u>0.459</u>	<u>0.435</u>

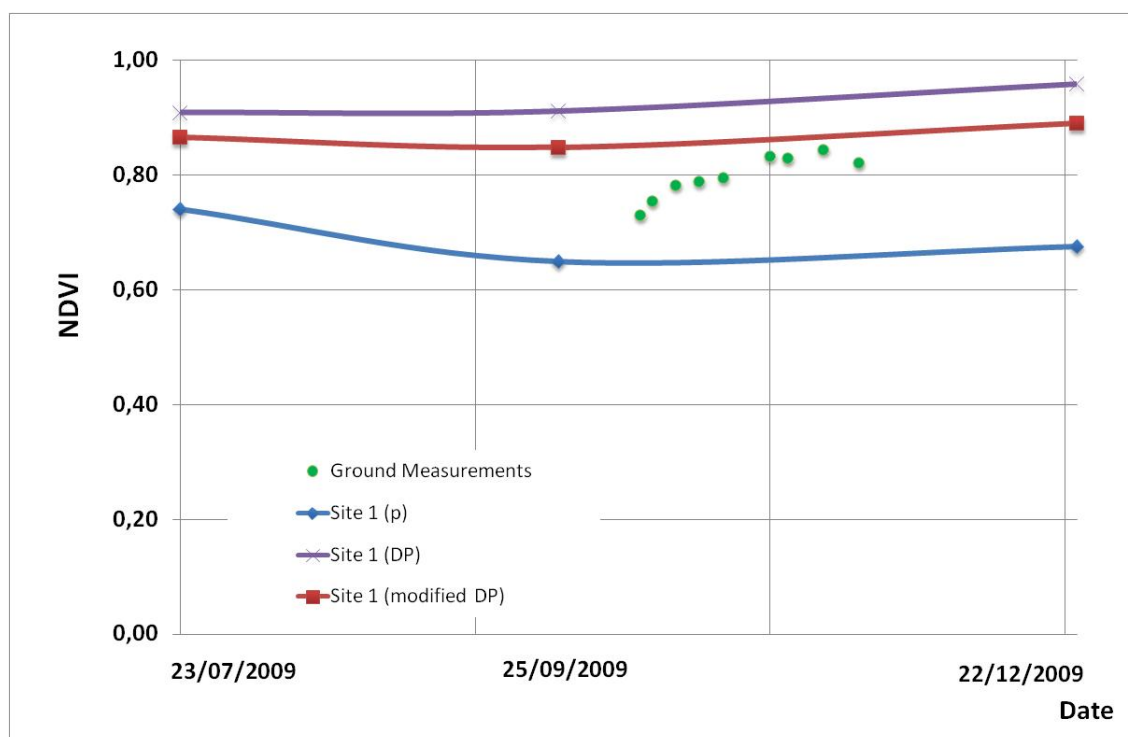
Figure 8. Comparison of NDVI values derived from satellite images (before and after atmospheric correction) and ground spectroradiometric measurements for Site 1.



In order to evaluate the effectiveness of the revised darkest pixel atmospheric correction, ground spectroradiometric measurements using the GER1500 field spectroradiometer from field campaigns were used. Figure 8 shows the results from field campaign at Site 1 during March 2010 (05/03/2009; 12/03/2009 and 24/03/2009). As is shown, ground spectroradiometric results are closer to atmospheric corrected NDVI values (using the DP and modified DP) in relation to NDVI values before atmospheric correction. Modified DP atmospheric correction tends to be most accurate compared to DP algorithm.

It is apparent that the difference of the NDVI results without atmospheric correction and ground measurements can be 15%. It is important to highlight that any omission of atmospheric effects may cause erroneous or non-qualitative outcomes regarding the presence of archaeological crop marks in the area of interest. Similarly, Figure 9 indicates the results obtained from an agricultural field near Paphos airport. Again, atmospheric corrected images match closely with spectroradiometer derived NDVI values.

Figure 9. Comparison of NDVI values derived from satellite images (before and after atmospheric correction) and ground spectroradiometric measurements for the agricultural site near Paphos airport.



6. Conclusions

Remote sensing archaeological investigations use not only up-to date satellite imagery, but also archived data. All these datasets should have, firstly, a radiometric correction, in order to retrieve valuable information. An important radiometric correction is the atmospheric correction which can be easily applied using image-based atmospheric corrections techniques, such as the simplest one, the DP algorithm. Most published atmospheric correction methods have been developed for specific targets, such as, coastal and inland waters or land, and their effectiveness for other targets and different applications needed first to be assessed [21,45,46]. Indeed, an example of how important the atmospheric correction is, for archaeological research, especially when NDVI's are used for archaeological crops detection, is shown in this study. It is considered that omissions in considering the effects of the atmosphere when vegetation indices from satellite images are used, may lead to major discrepancies in the final estimation of evapotranspiration. The absence of such considerations as the effect of the atmosphere, when NDVI's are used in archaeological research, is demonstrated by this study.

This paper highlights the importance of atmospheric correction of satellite images intended for archaeological research. For this reason atmospheric and non-atmospheric correction images were used in order to evaluate the importance of this procedure. A simple atmospheric correction algorithm was used (modified DP algorithm), which is considered to provide a credible correction, at least for cloud-free skies. Indeed, ground spectroradiometric measurements were acquired at a dark target (Asprokremmos Dam) and their “true” reflectance was estimated.

The NDVI diagram was evaluated for archaeological and non-archaeological areas and it was shown that errors might occur if atmospheric corrections are ignored (0.06). However, although NDVI differences are ignored in archaeological research studies, the impact of atmospheric correction should not be, since NDVI equation is a ratio of Red and NIR bands and therefore the atmospheric correction is minimized. In cases such as SR index (Red/NIR band), the differences before and after the atmospheric correction are estimated to be much more. The diagram showed that the general trend of the NDVI from the phenological cycle of the crops remains the same without any atmospheric corrections. However, if absolute values are needed for comparison between two different dates, then atmospheric correction procedures should first be applied.

The authors explored the importance of considering any available meteorological data, such as, RH values during the satellite overpass so as to be able to investigate any water vapor effects in the NIR region. DP atmospheric correction was found to have suffered sometimes in the NIR, due to the water vapor absorption. Indeed, during the application of the revised DP atmospheric correction, optical thickness values of water vapor were retrieved for all images in the dataset. A known archaeological crop mark and a dark target were used in order to evaluate the quality of the image for each band (Vis-NIR bands). All image histograms were linearly stretched to common min and max values and then visual interpretation was performed. The interpretation showed that in cloud-free images with low water vapor optical thickness ($\approx < 0.05$), atmospheric correction can increase the quality of the satellite image and therefore improve the interpretation.

Based on the fact that NDVI has been widely used in several applications, especially for archaeological research purposes, the mean difference of 15% between the atmospheric and non-atmospheric corrected values has a significant meaning. Indeed, for the purposes in which NDVI is used, the effects of the atmosphere must be taken into account. Otherwise, the retrieved outcomes will not lead to the retrieval of any crop marks and may well lead to erroneous results. The proposed revised DP atmospheric correction is simple and can be easily used by remote sensing users and archaeologists for areas of interest which may consist of large water bodies such as water reservoirs or dams to be used as suitable dark targets. The dam reflectance values provided in the *in situ* study can be used as standard reflectance values by any other users in the Mediterranean region during the application of the modified DP atmospheric correction.

Acknowledgments

The authors would like to express their appreciation to the Alexander Onassis Foundation for funding the PhD study of Athos Agapiou. Publication fees are funded from the Cyprus University of Technology. Thanks are given to the Remote Sensing Laboratory of the Department of Civil Engineering & Geomatics at the Cyprus University of Technology for the support. Special thanks are

given to the USGS Glovis for providing the Landsat TM/ETM+ data and to Meteorological Service of Cyprus for the meteorological data from Paphos automatic meteorological station. Also thanks are given to Costas Tsiartas for editing the paper.

References

1. Siart, C.; Eitel, B.; Panagiotopoulos, D. Investigation of past archaeological landscapes using remote sensing and GIS: A multi-method case study from Mount Ida, Crete. *J. Archaeol. Sci.* **2008**, *35*, 2918-2926.
2. Masini, N.; Lasaponara, R. Investigating the spectral capability of QuickBird data to detect archaeological remains buried under vegetated and not vegetated areas. *J. Cult. Herit.* **2007**, *8*, 53-60.
3. Alexakis, D.; Sarris, A.; Astaras, T.; Albanakis, K. Detection of neolithic settlements in Thessaly (Greece) through multispectral and hyperspectral satellite imagery. *Sensors* **2009**, *9*, 1167-1187.
4. Agapiou, A.; Hadjimitsis, G.D.; Sarris, A.; Themistocleous, K.; Papadavid, G. Hyperspectral Ground Truth Data for the Detection of Buried Architectural Remains. In *Proceedings of 3rd International Euro-Mediterranean Conference (EuroMed 2010)*, Limassol, Cyprus, 8–13 November 2010; Lecture Notes of Computer Science; Volume 6436, pp. 318-331.
5. Alexakis, A.; Sarris, A.; Astaras, T.; Albanakis, K. Integrated GIS, remote sensing and geomorphologic approaches for the reconstruction of the landscape habitation of Thessaly during the neolithic period. *J. Archaeol. Sci.* **2011**, *38*, 89-100.
6. Alexakis, D.; Sarris, A. Environmental and Human Risk Assessment of the Prehistoric and Historic Archaeological Sites of Western Crete (Greece) with the Use of GIS, Remote Sensing, Fuzzy Logic and Neural Networks. In *Proceedings of 3rd International Euro-Mediterranean Conference (EuroMed 2010)*, Limassol, Cyprus, 8–13 November 2010; Lecture Notes of Computer Science; Volume 6436, pp. 332-342.
7. Hadjimitsis, D.G.; Themistocleous, K.; Agapiou, A.; Clayton, C.R.I. Multi-temporal study of archaeological sites in Cyprus using atmospheric corrected satellite remotely sensed data. *Int. J. Archit. Comput.* **2009**, *7*, 121-138.
8. Kincey, M.; Challis, K. Monitoring fragile upland landscapes: The application of airborne lidar. *J. Nature Conserv.* **2010**, *18*, 126-134.
9. Hadjimitsis, D.G.; Agapiou, A.; Alexakis, D.; Sarris, A. Exploring natural and anthropogenic hazard risk for cultural heritage in Cyprus using remote sensing and GIS. *Int. J. Dig. Earth* **2011**, doi:10.1080/17538947.2011.602119.
10. Sharpe, L. Geophysical, Geochemical and Arable Crop Responses to Archaeological Sites in the Upper Clyde Valley, Scotland. Ph.D. Thesis, Department of Archaeology, Faculty of Physical Sciences, University of Glasgow, Glasgow, UK, 2004.
11. Adqus, S.A.; Hanson, W.S.; Drummond, J. A Comparative Study for Finding Archaeological Crop Marks using Airborne Hyperspectral, Multispectral and Digital Photographic Data. In *Proceedings of the 2007 Annual Conference of the Remote Sensing and Photogrammetry Society*, Newcastle, UK, 11–15 October 2009; pp.361-365.

12. Lasaponara, R.; Masini, N. Detection of archaeological crop marks by using satellite QuickBird multispectral imagery. *J. Archaeol. Sci.* **2007**, *34*, 214-221.
13. Rowlands, A.; Sarris, A. Detection of exposed and subsurface archaeological remains using multi-sensor remote sensing. *J. Archaeol. Sci.* **2007**, *34*, 795-803.
14. Agapiou, A.; Hadjimitsis, D. Vegetation indices and field spectroradiometric measurements for validation of buried architectural remains: Verification under area surveyed with geophysical campaigns. *J. Appl. Remote Sens.* **2011**, doi:10.1117/1.3645590.
15. Lillesand, T.M.; Kiefer, R.W.; Chipman, J.W. *Remote Sensing and Image Interpretation*; Wiley: Hoboken, NJ, USA, 2004.
16. Duggin, M.J.; Piwinski, D. Recorded radiance indices for vegetation monitoring using NOAA AVHRR data; atmospheric and other effects in multitemporal data sets. *Appl. Optics* **1984**, *23*, 2620-2623.
17. Honkavaara, E.; Arbiol, R.; Markelin, L.; Martinez, L.; Cramer, M.; Bovet, S.; Chandelier, L.; Ilves, R.; Klonus, R.; Marshal, P.; Schläpfer, D.; Tabor, M.; Thom, C.; Veje, N. Digital airborne photogrammetry—A new tool for quantitative remote sensing?—A state-of-the-art review on radiometric aspects of digital photogrammetric images. *Remote Sens.* **2009**, *1*, 577-605.
18. Bagheri, S. Nearshore water quality estimation using atmospherically corrected AVIRIS data. *Remote Sens.* **2011**, *3*, 257-269.
19. Song, C.; Woodcock, E.C. Monitoring forest succession with multitemporal Landsat images: Factors of uncertainty. *IEEE Trans. Geosci. Remote Sens.* **2003**, *41*, 2557-2567.
20. Che, N.; Price, J.C. Survey of Radiometric calibration results and methods for visible and near infrared channels of NOAA-7, -9, and -11 AVHRRs. *Remote Sens. Environ.* **1992**, *41*, 19-27.
21. Hadjimitsis, D.G.; Papadavid, G.; Agapiou, A.; Themistocleous, K.; Hadjimitsis, M.G.; Retalis, A.; Michaelides, S.; Chrysoulakis, N.; Toullos, L.; Clayton, C.R.I. Atmospheric correction for satellite remotely sensed data intended for agricultural applications: Impact on vegetation indices. *Natural. Hazards Earth Syst. Sci.* **2010**, *10*, 89-95.
22. Bastiaanssen, W.G.M.; Molden, D.J.; Makin, I.W. Remote sensing for irrigated agriculture: Examples from research and possible applications. *Agr. Water Manage.* **2000**, *46*, 137-155.
23. Kaufman, Y.J.; Sendra, C. Algorithm for automatic corrections to visible and near-IR satellite imagery. *Int. J. Remote Sens.* **1988**, *9*, 1357-1381.
24. Courault, D.; Seguin, B.; Olioso, A. Review to Estimate Evapotranspiration from Remote Sensing Data: Some Examples from the Simplified Relationship to the Use of Mesoscale Atmospheric Models. Presented at *ICID International Workshop on Remote Sensing of ET for Large Regions*, Montpellier, France, 17 September 2003.
25. Hadjimitsis, D.G.; Clayton, C.R.I.; Hope, V.S. An assessment of the effectiveness of atmospheric correction algorithms through the remote sensing of some reservoirs. *Int. J. Remote Sens.* **2004**, *25*, 3651-3674.
26. Hadjimitsis, D.G.; Clayton, C.R.I.; Hope, V.S. The Importance of Accounting for Atmospheric Effects in Satellite Remote Sensing: A Case Study from the Lower Thames Valley Area, UK. In *Proceedings of Space 2000: The Seventh International Conference and Exposition on Engineering, Construction, Operations, and Business in Space. ASCE Conference on Space and Robotics*, Albuquerque, NM, USA, 27 February–2 March 2000; pp. 194-201.

27. Hadjimitsis, D.G.; Clayton, C.R.I.; Retalis, A. On the darkest pixel atmospheric correction algorithm: A revised procedure for environmental applications of satellite remotely sensed imagery. *Proc. SPIE* **2004**, 5239, 464-471.
28. Lu, D.; Mausel, P.; Brondizio E.; Moran, E. Assessment of atmospheric correction methods for Landsat TM data applicable to Amazon basin LBA research. *Int. J. Remote Sens.* **2002**, 23, 2651-2671.
29. Hadjimitsis, D.G.; Clayton, C.R.I. The application of the covariance matrix statistical method for removing atmospheric effects from satellite remotely sensed data intended for environmental applications. *Proc. SPIE* **2004**, doi:10.1117/12.751887.
30. Hadjimitsis, D.G.; Clayton, C.R.I. The use of an improved atmospheric correction algorithm for removing atmospheric effects from remotely sensed images using an atmosphere-surface simulation and meteorological data. *Meteorol. Appl.* **2008**, 15, 381-387.
31. Hadjimitsis, D.G.; Clayton, C.R.I. Field spectroscopy for assisting water quality monitoring and assessment in water treatment reservoirs using atmospheric corrected satellite remotely sensed imagery. *Remote Sens.* **2011**, 3, 362-377.
32. Song, J.; Duanjun, L.; Wesely, M.L. A simplified atmospheric correction procedure for the Normalized Difference Vegetation Index. *Photogramm. Eng. Remote Sensing*, **2003**, 69, 521-528.
33. Chrysoulakis, N.; Abrams, M.; Feidas, H.; Arai, K. Comparison of atmospheric correction methods using ASTER data for the area of Crete: The ATMOSAT Project. *Int. J. Remote Sens.* **2010**, 31, 6347-6385.
34. Forster, C.B. Derivation of atmospheric correction procedures for LANDSAT MSS with particular reference to urban data. *Int. J. Remote Sens.* **1984**, 5, 799-817.
35. Iacovou, M.; Stylianidis, E.; Sarris, A.; Agapiou, A. A Long-Term Response to the Need to Make Modern Development and the Preservation of the Archaeo-Cultural Record Mutually Compatible Operations: The GIS Contribution. In *Proceedings of the 22nd CIPA Symposium, Digital Documentation, Interpretation & Presentation of Cultural Heritage*, Kyoto, Japan, 11–15 October 2009.
36. Agapiou, A.; Iacovou, M.; Sarris, A. Spatial Analysis of the Archaeological Sites of the Palaepaphos Region (Northwest Cyprus), during the 3rd and 2nd Millennium BC Using GIS. In *Proceedings of The XXXVIII Annual Conference on Computer Applications and Quantitative Methods in Archaeology, CAA*, Granada, Spain, 6–9 April 2010; in press.
37. Iacovou, M. *The Palaepaphos Urban Landscape Project: Theoretical Background and Preliminary Report 2006-2007*; Report of Department of Antiquities Cyprus; Department of Antiquities: Nicosia, Cyprus, 2008; pp. 263-289.
38. Sarris, A.; Kokkinou, E.; Soupios, P.; Papadopoulos, E.; Trigkas, V.; Sepsa, U.; Gionis, D.; Iacovou, M.; Agapiou, A.; Satraki, A.; Stylianides, St. Geophysical Investigations at Palaipaphos, Cyprus. In *Proceedings of the 36th Annual Conference on Computer Applications and Quantitative Methods in Archaeology, CAA, On the Road to Reconstructing the Past*, Budapest, Hungary, 2–6 April 2008.
39. Maier, F.G.; Karageorghis, V. *Paphos, History and Archaeology*; A.G. Leventis Foundation: Nicosia, Cyprus, 1984.

40. Hantson, S.; Chuvieco, E. Evaluation of different topographic correction methods for Landsat imagery. *Int. J. Appl. Earth Obs. Geoinf.* **2011**, *13*, 691-700.
41. Papoutsas, C.; Hadjimitsis, D.G.; Alexakis, D. Characterizing the spectral signatures and optical properties of dams in Cyprus using field spectroradiometric measurements. *Proc. SPIE* **2011**, doi:10.1117/12.898353.
42. McClatchey, R.A.; Fenn, W.S.; Selby, J.E.A.; Volz, F.E.; Garing, J.S. *Optical Properties of the Atmosphere*; Rep. AFCr1-71-0279, 85; Air Force Cambridge Res. Lab.: Bedford, MA, USA, 1984.
43. Pinty, B.; Verstraete, M.M. GEMI: A nonlinear index to monitor global vegetation from satellites. *Vegetation* **1992**, *101*, 15-20.
44. Kaufman, Y.J.; Tanré, D. Atmospherically resistant vegetation index (ARVI). *IEEE Trans. Geosci. Remote Sens.* **1992**, *30*, 261-270.
45. Hadjimitsis, D.G.; Clayton, C.R.I. Assessment of temporal variations of water quality in inland water bodies using atmospheric corrected satellite remotely sensed image data. *Environ. Monit. Assess.* **2009**, *159*, 281-292.
46. Hadjimitsis, D.G.; Clayton, C.R.I.; Retalis, A. The use of selected pseudo-invariant targets for the application of atmospheric correction in multi-temporal studies using satellite remotely sensed imagery. *Int. J. Appl. Earth Obs. Geoinf.* **2009**, *11*, 192-200.

© 2011 by the authors; licensee MDPI, Basel, Switzerland. This article is an open access article distributed under the terms and conditions of the Creative Commons Attribution license (<http://creativecommons.org/licenses/by/3.0/>).